

Fast Surrogate Models for Adaptive Aircraft Trajectory Prediction in En route Airspace

Nick Pepper ^{*}

The Alan Turing Institute, London, England NW1 2DB, United Kingdom

Marc Thomas [†]

NATS, Fareham, England PO15 7FL, United Kingdom

Zack Xuereb Conti [‡]

The Alan Turing Institute, London, England NW1 2DB, United Kingdom

Trajectory prediction (TP) is crucial for ensuring safety and efficiency in modern air traffic management systems. It is, for example, a core component of conflict detection and resolution tools, arrival sequencing algorithms, capacity planning, as well as several future concepts. However, TP accuracy within operational systems is hampered by a range of epistemic uncertainties such as the mass and performance settings of aircraft and the effect of meteorological conditions on aircraft performance. It can also require considerable computational resources.

This paper proposes a method for adaptive TP that has two components: first, a fast surrogate TP model based on linear state space models (LSSMs) with an execution time that was 6.7 times lower on average than an implementation of the Base of Aircraft Data (BADA) in Python. It is demonstrated that such models can effectively emulate the BADA aircraft performance model, which is based on the numerical solution of a partial differential equation (PDE), and that the LSSMs can be fitted to trajectories in a dataset of historic flight data. Secondly, the paper proposes an algorithm to assimilate radar observations using particle filtering to adaptively refine TP accuracy. Comparison with baselines using BADA and Kalman filtering demonstrate that the proposed framework improves system identification and state estimation for both climb and descent phases, with 46.3% and 64.7% better estimates for time to top of climb and bottom of descent compared to the best performing benchmark model. In particular, the particle filtering approach provides the flexibility to capture non-linear performance effects including the CAS-Mach transition.

Nomenclature

A. BADA parameters

h	= Geodetic altitude
$\frac{dh}{dt}$	= Rate of climb/descent
T	= ISA temperature
ΔT	= Temperature correction
D	= Aircraft drag
V_{TAS}	= True airspeed
m	= Aircraft mass
g_0	= Gravitational acceleration
f	= Energy share factor
M	= Mach number

^{*}Senior Research Associate, The Alan Turing Institute, London, England NW1 2DB, United Kingdom

[†]Researcher, Department of Research and Development, NATS; also Visiting Professor, Queen Mary University London

[‡]Research Fellow, The Alan Turing Institute, London, England NW1 2DB, United Kingdom

B. Linear state space models

A	=	Continuous time dynamics matrix
B	=	Continuous time input matrix
Φ_A	=	Discrete time dynamics matrix
Φ_B	=	Discrete time input matrix
x	=	State vector
u	=	Input vector
L	=	Matrix of scaling factors
θ	=	LSSM parameters

C. Particle filter parameters

w	=	Particle weight
n_{eff}	=	Effective particle number
a	=	Shrinkage parameter

D. Kalman filter parameters

P	=	State uncertainty matrix
Q	=	Process noise matrix
R	=	Measurement noise covariance
$\alpha_p, \alpha_q, \alpha_b$	=	Scaling terms

I. Introduction

Trajectory prediction (TP) is utilised in operational air traffic management systems to underpin traffic load prediction, short and medium term conflict detection, and many other functions. Models such as the Base of Aircraft Data (BADA) model are deterministic trajectory prediction models calibrated to produce generic aircraft performance [1]. Accurate trajectory prediction with deterministic methods is hampered by the presence of significant epistemic uncertainties. For example the mass and performance settings of aircraft are not known to the air traffic control officer (ATCO) [2], while meteorological conditions are uncertain and can have a significant effect on aircraft performance [3]. These epistemic uncertainties can cause significant misspecification between predicted and observed trajectories.

In order to address this issue, many works have explored leveraging large datasets of available trajectory data in order to improve TP using data-driven methods to approach TP as a sequence-to-sequence learning task. Investigated methods include Long-Short Term Memory networks [4, 5], Convolutional Neural Networks [6], Generative Adversarial Networks [7], and Hidden Markov Models [8]. Such methods tend to be applied to terminal airspace, where there is less diversity in followed routes compared to en route airspace. As an alternative to data-driven TP using deterministic data-driven methods, probabilistic methods have been proposed such that predicted trajectories can be obtained through sampling and in principle, credible intervals could be computed to indicate the level of uncertainty in the prediction [9–11]. This is useful in the setting of conflict detection, where TP methods are often used to identify regions of airspace an aircraft may plausibly occupy within a time interval, which is based on applying conservative bounds around a deterministic prediction to account for model misspecification (see, e.g. [12–14]).

As an alternative to improving the fidelity of the TP model, there have been a number of works that seek to assimilate live trajectory data to improve an existing TP model. For instance Lymeropoulos [15] implemented a sequential conditional particle filter to update trajectory predictions of aircraft in cruise subject to uncertainty arising from wind conditions. Similarly, algorithms have been proposed to estimate aircraft takeoff mass, which is unknown to the ATCO and has a significant effect on climb performance, from trajectory data (see, e.g. [16–18]). These methods have the advantage of continuously refining predictions based on observations of a trajectory. However, a drawback is that sequential Monte Carlo methods require numerous evaluations of a deterministic TP model such as BADA, which can require considerable computational resources when scaled to hundreds of aircraft within a real-world airspace, even though an individual model evaluation may only be of the order of milliseconds. Instead, the existing TP model could

be substituted with a fast surrogate model. This would allow rapid sampling for Bayesian assimilation of observed trajectory data, while also enabling probabilistic TP by generating trajectory samples inexpensively.

While Kalman filters are widely used for aircraft tracking (see, e.g. [19]) they are not necessarily appropriate for the task of system identification of a TP model. Identifying the underlying aircraft dynamics is more challenging than estimating an aircraft's position because of switching between various modes of climb and descent within the same trajectory. Examples of discontinuous changes in aircraft dynamics include the CAS-Mach transition or when aircraft enter a region of turbulence. Aircraft performance in descent is often influenced by level-by constraints in the clearances issued by ATCOs. This means that the dynamical model best describing an aircraft's trajectory can change discontinuously between observations. A single Kalman filter is often unable to track systems with such mode switching behaviour [20]. For this reason more flexible approaches employing particle filtering [21] or mixtures of linear systems [14] and TP models [22] have previously been investigated.

In the proposed method fast sampling is achieved by modelling variations of true airspeed (TAS) and geodetic altitude in climb as a discrete-time linear (time-invariant) state space model (LSSM), while a Sequential Monte Carlo (SMC) method is used as a flexible means of assimilating observations of aircraft trajectories in real time. More specifically, a Liu and West particle filter is implemented for the assimilation as a specialized SMC algorithm for joint state estimation and system identification [23]. A sampling based approximation of the prior distribution for the uncertain aircraft dynamics is formed by fitting LSSMs to a training dataset of trajectory data in an optimization process. The proposed methodology for adaptive TP, which has been developed specifically for online trajectory prediction within a Digital Twin of enroute airspace [24], offers several features:

- A fast surrogate for BADA trajectories using LSSMs fitted in an optimization process
- A framework for assimilation of trajectory data based on particle filtering that has the flexibility to handle non-linear changes in aircraft dynamics, as occurs at the CAS-Mach transition for instance
- An improved mean prediction of the top of climb point through assimilation of trajectory data
- An ensemble TP through sampling of particles in the filter that may be used to compute credible intervals for the TP

The remainder of this paper follows the following structure: Section II.A describes the proposed fast LSSM surrogate as a substitute for BADA and optimization process for fitting trajectory data. Section II.B outlines the steps of the particle filter approach used to assimilate trajectory observations as they become available and update an ensemble trajectory prediction. Section III outlines the datasets used to fit LSSMs to form a prior on the system dynamics and the held out dataset used to test the effectiveness algorithm. Finally, section IV presents the results of applying the proposed algorithm to the held out dataset, baselines by BADA and some standard data-driven approaches.

II. Methodology

A. State-space modelling of the BADA equations

The Base of Aircraft Data (BADA) is a total-energy model that uses a physics-based model to predict aircraft trajectories for a range of aircraft types. The model is based around a PDE that balances work done by the aircraft thrust against changes in gravitational potential energy and kinetic energy. By assuming either a constant calibrated airspeed (CAS) or constant Mach speed with altitude, an equation for rate of climb or descent (ROCD) can be defined [1]:

$$\frac{dh}{dt} = \frac{T - \Delta T}{T} \left[\frac{(T_{HR} - D)V_{TAS}}{mg_0} \right] f(M), \quad (1)$$

where h denotes altitude, $\frac{dh}{dt}$ denotes the ROCD, T_{HR} the aircraft thrust, V_{TAS} the TAS, and $f(\cdot)$ the energy share factor (ESF), defined as a function of the Mach number, M . The ESF governs the tradeoff between changes in gravitational potential energy and kinetic energy. It has a different functional form depending on whether the aircraft is flying at constant CAS or Mach speed. Additionally, T represents air temperature in the International Standard Atmosphere (ISA) model and ΔT a temperature correction that may be applied to BADA, although in what follows this is set to 0.

Many of the terms in (1) are functions of h and V_{TAS} . For instance, T varies with h in the ISA model while in BADA T_{HR} is a function of h for jet aircraft and both h and V_{TAS} for turboprop aircraft. Similarly, D is a function of V_{TAS}^2 but also has further dependence on h and V_{TAS} through the aerodynamic coefficients. Lastly, $f(\cdot)$ is a four branch function where each branch is a function of M , which itself can be defined as a conversion from V_{TAS} at a specific h .

We define a linear time-invariant (LTI) model for climbing aircraft, with a two-dimensional state vector including the geodetic altitude, and TAS, denoted $\mathbf{x} = [h, V_{TAS}]^\top$. These quantities are selected as the minimum set of variables

required by BADA. The continuous time state-space equation for this system is defined as:

$$\dot{\mathbf{x}} = A\mathbf{x} + B\mathbf{u}, \quad (2)$$

where $A \in \mathbb{R}^{2 \times 2}$ is the dynamics matrix, $B \in \mathbb{R}^{2 \times 2}$ is the input matrix, and $\mathbf{u} \in \mathbb{R}^2$ is the input (or control) vector. (2) is a continuous-time model. However, radar measurements are available at discrete times, for instance Mode S radar returns refresh every 6s. For this reason the discrete time formulation of (2) is used:

$$\mathbf{x}^{(t+1)} = \Phi_A \mathbf{x}^{(t)} + \Phi_B \mathbf{u}_t, \quad (3)$$

where Φ_A and Φ_B , the discrete time versions of A and B respectively, are computed from A , assuming it is invertible, via:

$$\Phi_A = e^{\Delta t A} \text{ and } \Phi_B = (\Phi_A - I_2)A^{-1}B, \quad (4)$$

where I_2 is a 2×2 identity matrix and radar blips are 6 seconds apart i.e. $\Delta t = 6$ s. Following the developments in Appendix V.A, it was found that the forcing term in the linearization of (1) was dependent on the state, rather than time. Rather than remove the forcing term entirely we retain a constant forcing operator, with (3) recast as:

$$\mathbf{x}^{(t+1)} = \Phi_A \mathbf{x}^{(t)} + \Phi_B. \quad (5)$$

The LSSM described by (5) can be interpreted as having a forcing applied from the aircraft thrust that increases both TAS and altitude (when flying at constant CAS), while the state space operator Φ_A describes the dynamics that govern the tradeoff between TAS and h , in a similar manner to the ESF in (1).

System identification was performed through an optimization procedure that determined the elements of Φ_A and Φ_B from trajectory data. Let the set of n radar returns that represent an aircraft trajectory, either obtained from real-world data or from solution of the BADA equations, be denoted $\mathbb{X} = [\mathbf{x}^{(1)}, \dots, \mathbf{x}^{(n)}]$. The fitted LSSM model for \mathbb{X} was found through solving the unconstrained optimization problem:

$$\hat{\theta} = \arg \min_{\theta} \mathcal{J}(\theta | \mathbb{X}), \quad (6)$$

where $\theta \in \mathbb{R}^6$ collects the elements of Φ_A and Φ_B . The cost function, $\mathcal{J}(\cdot)$ is defined as:

$$\mathcal{J}(\theta | \mathbb{X}) = \sum_{i=2}^n (\hat{\mathbf{x}}^{(i)} - \mathbf{x}^{(i)})^\top L^{-2} (\hat{\mathbf{x}}^{(i)} - \mathbf{x}^{(i)}), \quad (7)$$

where $L \in \mathbb{R}^{2 \times 2}$ is a diagonal matrix containing scaling factors. In this work 30,000 ft and 400 kts were used as scaling factors, reflecting typical cruising altitude and groundspeed for jet engined aircraft in en route airspace. The set $\hat{\mathbb{X}} = [\mathbf{x}^{(1)}, \hat{\mathbf{x}}^{(2)}, \dots, \hat{\mathbf{x}}^{(n)}]$ is generated by initializing at $\mathbf{x}^{(1)}$ (the first radar blip in \mathbb{X}) and recursively applying Φ_A and Φ_B , as in (3). Given that the derivatives of $\mathcal{J}(\theta | \mathbb{X})$ with respect to θ are non-trivial due to the recursive summation in $\hat{\mathbb{X}}$, the Nelder-Mead algorithm, a non-convex optimization method, was used to solve (6) [25].

Figure 1 shows the result of applying the LSSM methodology described here to emulate the trajectories in BADA of commonly occurring aircraft in UK airspace. The selected aircraft types contain a mix of ICAO wake turbulence categories and engine types. Trajectory data, \mathbb{X} , is generated using BADA for climbs and descents between flight level 210 (21,000 ft at standard atmospheric pressure) and either the geodetic altitude corresponding to the tropopause or 5,000 ft above the CAS-Mach transition point. In Figure 1 the BADA trajectories are solid lines, while dashed lines indicate the trajectories generated from recursively applying the LSSMs ($\hat{\mathbb{X}}$). As can be seen from the figure, there is a high degree of agreement between the two set of trajectories. However, the trajectories from the LSSMs are less expensive to generate as they do not require (1) to be solved numerically.

Table 5 indicates the root mean square error between the trajectories derived from BADA versus those from the fitted LSSMs for the aircraft types in Figure 1 in climb. Using the initial conditions for the B738 to normalise the scales for altitude and airspeed (210,000 ft and 400 kts), these errors can be expressed as a percentage. It was found that the percentage error of the LSSM surrogates is very low: 0.021% error in the geodetic altitude and 0.028% for TAS. Similarly, Table 6 displays the results of the fitting for BADA trajectories in descent. Comparing the data in Tables 5 and 6, the mean fitting error is generally worse for descent. For trajectory segments above the transition point this is likely because the descending trajectories are longer due to the transition point being lower in descent, hence the descents accumulate more error. Below the transition point, the mean error in descent is raised by the outlier of the

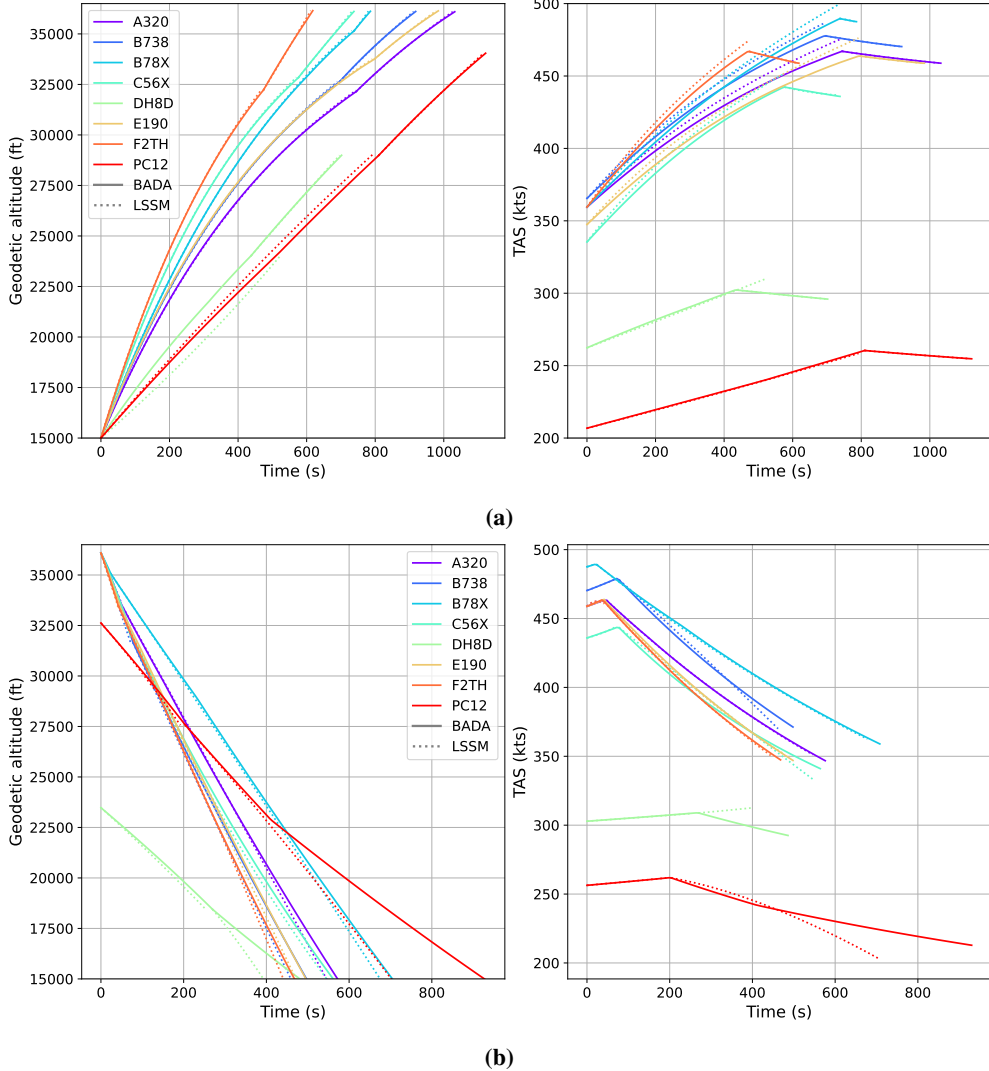


Fig. 1 Fitted LSSMs used as an emulator for the trajectories of a range of climbing and descending aircraft in the BADA model.

PC12 aircraft type. The parameters of the PC12 in BADA are such that there is a discontinuous change in the thrust profile around FL 230. As a consequence, the PC12 trajectory is piecewise linear below the transition point, which cannot be well approximated using a single LSSM. Lastly, Tables 5 and 6 show the relative difference in execution time between the Python implementation of BADA used and the fitted LSSMs, with the LSSMs faster by a factor of 5.26 in climb and 8.11 in descent (descending trajectories were generally longer than climbs).

Aircraft type	Below CAS-Mach transition		Above CAS-Mach transition		Execution time (ms)		
	Δh (ft)	ΔV_{TAS} (kts)	Δh (ft)	ΔV_{TAS} (kts)	BADA	LSSM	BADA/LSSM
A320	31.29	5.43	23.57	0.00	5.72	0.93	6.15
B738	34.73	5.41	26.64	0.00	4.67	0.87	5.37
B78X	43.15	6.12	61.05	0.10	3.54	0.70	5.07
C56X	44.54	5.56	44.53	0.32	3.35	0.64	5.26
DH8D	1362.43	0.88	36.46	0.00	3.17	0.71	4.44
E190	29.94	7.15	28.95	0.00	4.58	0.85	5.40
F2TH	48.31	4.56	60.79	0.03	2.75	0.53	5.15
PC12	302.42	0.41	30.77	0.00	4.83	0.93	5.21
Mean	237.10	4.44	39.10	0.06	4.07	0.77	5.26

Table 5 Root mean square error between BADA trajectories and those generated from the fitted LSSMs for aircraft in climb.

Aircraft type	Below CAS-Mach transition		Above CAS-Mach transition		Execution time (ms)		
	Δh (ft)	ΔV_{TAS} (kts)	Δh (ft)	ΔV_{TAS} (kts)	BADA	LSSM	BADA/LSSM
A320	300.09	0.23	38.04	1.13	4.20	0.57	7.36
B738	740.26	3.38	272.22	0.02	4.87	0.62	7.89
B78X	330.64	0.80	171.34	0.01	7.53	0.88	8.59
C56X	345.38	4.24	259.19	0.32	4.65	0.65	7.16
DH8D	778.10	7.95	190.10	0.08	5.59	0.63	8.83
E190	401.66	0.73	223.11	0.10	5.00	0.65	7.68
F2TH	375.93	0.56	32.27	1.10	3.77	0.53	7.18
PC12	1519.78	8.34	148.32	0.02	15.72	1.54	10.23
Mean	598.98	3.28	166.82	0.35	6.42	0.76	8.11

Table 6 Root mean square error between BADA trajectories and those generated from the fitted LSSMs for aircraft in descent.

B. Particle filtering

Repeating the optimization procedure in (6) for a dataset of n_t trajectories, denoted $\mathbb{T} = [\mathbb{X}^{(1)}, \dots, \mathbb{X}^{(n_t)}]$, yields a set of n_t optimal LSSMs, which we denote $\mathbb{S} = [(\Phi_A, \Phi_B)^{(1)}, \dots, (\Phi_A, \Phi_B)^{(n_t)}]$. The LSSMs are optimal in the sense that they are the predictors that most closely match the trajectories in \mathbb{T} . The trajectories in \mathbb{T} and LSSMs in \mathbb{S} are specific to an aircraft type. The LSSMs in \mathbb{S} can be thought of as a set of samples drawn from the prior distribution for θ , $p(\theta)$. As more observations of an unseen trajectory become available, a particle filter approach is used to jointly estimate both the state of the aircraft, $p(\mathbf{x}|\mathbf{y}^{(1)}, \dots, \mathbf{y}^{(t)})$, and identify the underlying dynamics of the trajectory $p(\theta|\mathbf{y}^{(1)}, \dots, \mathbf{y}^{(t)})$, where $\mathbf{y}^{(i)}$ denotes an observation of altitude and TAS from the i^{th} radar blip in the trajectory and recalling from the previous sections that θ collects the elements of Φ_A and Φ_B . At a given timestep t , we wish to estimate the future states of the aircraft and the associated uncertainty.

A Liu and West particle filter (LWPF) [23] was implemented as a specialized method for joint state estimation and system identification. The Liu and West filter differs from methods such as the Interacting Multiple Model (IMM) approach in that it admits continuous system parameters, θ [26]. In contrast, approaches such as IMM filter from a discrete set of LSSMs in parallel which might limit the ability of the filter to assimilate radar observations if the underlying system parameters are not present in the set of models. The primary steps of the algorithm are summarized below, the interested reader is referred to Liu and West [23] and Nemeth et al [27] for more details on the method. In what follows, $\mathbf{x}^{(0)}$ denotes an initial observation of the aircraft's state which is used to initialise the filter. The prior distribution $p(\mathbf{x}^{(0)})$ represents the uncertainty in the initial state given measurement error. As is discussed in the context of Kalman filtering in Appendix V.B, this uncertainty is significantly smaller than the uncertainty surrounding the system dynamics. The main steps of the proposed adaptive trajectory prediction algorithm can be summarized as:

0) Sampling

Draw n_p samples from the prior distribution for $p(\mathbf{x}^{(0)})$ and sample from \mathbb{S} with replacement n_p times to obtain a set of particles with a state and LSSM associated with each. Initialize the particle weights, $\mathbf{w}^{(0)} = \mathbf{1}/n_p$.

1) Prediction

Evolve the state of each particle using the associated LSSM using (5).

2) Shrink system parameters towards the mean

Compute average system parameter from weighted sum of particles:

$$\bar{\theta} = \sum_{i=1}^{n_p} \mathbf{w}_i^{(t-1)} \theta_i^{(t-1)}, \quad (8)$$

together with the variance of system parameters in the filter:

$$V^{(t-1)} = \sum_{i=1}^{n_p} \mathbf{w}_i^{(t-1)} (\theta_i^{(t-1)} - \bar{\theta}) (\theta_i^{(t-1)} - \bar{\theta})^\top, \quad (9)$$

to yield the updated system parameters using associated with the i^{th} particle:

$$\theta_i^{(t)} = a \theta_i^{(t-1)} + (1 - a) \bar{\theta} + N(\mathbf{0}, b^2 V^{(t-1)}), \quad (10)$$

where $a = 1 - b^2$, which controls shrinkage towards $\bar{\theta}$. We achieved best results using $b = 0.2$.

3) Update particle states and weights

Using the measurement $\mathbf{y}^{(t)}$, compute the observation likelihood for each particle through:

$$p(\mathbf{y}^{(t)} | \mathbf{x}_i^{(t)}, \theta_i^{(t)}) = e^{-\frac{1}{2} ((\mathbf{y}^{(t)} - \mathbf{x}_i^{(t)})^\top R^{-1} (\mathbf{y}^{(t)} - \mathbf{x}_i^{(t)}))}, \quad (11)$$

where $\mathbf{x}_i^{(t)}$ denotes the state of the i^{th} particle at timestep t and $\theta_i^{(t)}$ the parameters of the LSSM associated with that particle. The matrix R is as defined in (7). The observation likelihood is used to update the normalized particle weight through:

$$w_i = \frac{p(\mathbf{y}^{(t)} | \mathbf{x}_i^{(t)}, \theta_i^{(t)})}{\sum_{j=1}^{n_p} p(\mathbf{y}^{(t)} | \mathbf{x}_j^{(t)}, \theta_j^{(t)})}. \quad (12)$$

4) Resampling

Resample the particle filter, where the probability of selecting the i^{th} particle is set to w_i . To avoid particle degeneracy, where weight is concentrated in only a few particles, resampling through stratified sampling is performed if the effective number of particles, n_{eff} , drops below a threshold. The effective number of particles is defined as:

$$n_{\text{eff}} = \frac{1}{\sum_{i=1}^{n_p} w_i^2}, \quad (13)$$

with the threshold below which stratified resampling is performed set to $0.5 \times n_p$. Occasionally aircraft will change their mode of climb or descent, leading to rapid changes in performance. This necessitated re-initialising the particle filter. This was triggered if the absolute difference between the estimated TAS and last observed TAS was greater than 5 knots.

5) State estimation

The filter state is the weighted sum of the states of individual particles, i.e.:

$$\hat{\mathbf{x}}^{(t)} = \sum_{i=1}^{n_p} w_i \mathbf{x}_i^{(t)}. \quad (14)$$

The estimated state of the filter is used to determine whether to perform ensemble trajectory prediction.

6) Ensemble Trajectory Prediction

If the estimated particle altitude, $\hat{\mathbf{x}}_1^{(t)}$, is equal to or greater than the aircraft's target altitude then cease iteration. Otherwise, a prediction for future states of the aircraft's climb is made using multinomial sampling from the particles. Initializing at $\mathbf{x}_i^{(t)}$, the LSSM associated with that particle is used to generate a predicted trajectory, $[\mathbf{x}_i^{(t)}, \mathbf{x}_i^{(t+1)}, \dots, \mathbf{x}_i^{(t+n)}]$. The mean and standard deviations of these samples can be used to return a deterministic TP together with a credible interval. The algorithm then returns to step 1.

III. Data preparation

A dataset consisting of 29 days' worth of Mode S radar surveillance data, collected from en route airspace in the UK in September 2019, was used to assess the effectiveness of the adaptive TP algorithm. The dataset was split into training, validation, and test sets in a 70/10/20 ratio. This resulted in 21 days of training data, 2 days of validation data, and 6 days of test data. The dataset was split based in this way to minimise data leakage between the train and test sets, particularly with regard to meteorological conditions.

The optimization process described in Section II.A was used to generate the set of LSSMs, \mathbb{S} , for the days in the training dataset. Table 7 displays the investigated aircraft types and the number of trajectories for each aircraft type in the various datasets. A range of aircraft types were investigated, from large passenger jets such as the B738 and A320 which are commonplace in UK airspace, to smaller business jets such as the C56X, and turboprop aircraft which are less frequently occurring and have markedly different performance characteristics to jet aircraft.

The performance of the particle filtering-based method for state estimation and trajectory prediction introduced in Section II.B was benchmarked against a simple method based on Kalman filtering. This simplistic trajectory prediction method assumes the aircraft will continue to climb or descend at the filtered ROCD and TAS and is outlined in Appendix V.B. The validation dataset was used to perform a sweep to set the hyperparameters of this method. Similarly, the number of particles used in the particle filter was selected based on a sweep of possible particle numbers. The results of this sweep are presented in Appendix V.C. Based on these results a maximum of 400 particles were used for each aircraft type (maximum because some aircraft types had fewer than 400 particles in their training datasets).

IV. Results

The adaptive TP algorithm presented in Section II.B was run over the trajectories in the test dataset for each aircraft type in Table 7. The accuracy of the proposed method was assessed by predicting the top of climb/bottom of descent point, in terms of the time taken to achieve that altitude and the distance flown while doing so. An ensemble of trajectories was generated by the LWPF, with the mean prediction of top of climb/bottom of descent of the samples compared against the test data. Three methods were used to benchmark the adaptive TP algorithm, two of which based around BADA, while the third was a simple benchmark employing Kalman filtering which is further described

Aircraft type	Engine type	Training trajectories		Validation trajectories		Test trajectories		Total	
		Climb	Descent	Climb	Descent	Climb	Descent	Climb	Descent
B738	Jet	16931	16476	1627	1622	4710	4526	23268	22624
A320	Jet	11198	12282	1050	1204	3169	3547	15417	17033
E190	Jet	2409	2443	160	174	715	701	3284	3318
C56X	Jet	342	372	36	40	108	101	486	513
B78X	Jet	61	61	5	6	15	12	81	79
DH8D	Turboprop	2660	1878	254	153	759	543	3673	2574
F2TH	Turboprop	162	216	18	16	53	58	233	290
PC12	Turboprop	121	94	19	19	37	32	177	145

Table 7 Number of trajectories in the train, validation, and test datasets for each aircraft type.

Method	MAE time error (s)		MAE distance error (nmi)	
	Climb	Descent	Climb	Descent
BADA ($t = 0$)	95.61	112.15	59.66	19.48
BADA	12.70	9.88	43.04	12.70
KF-TP	9.66	18.59	7.70	14.26
LWPF	5.19	6.56	3.94	4.27

Table 8 MAE to time and location of climb/bottom of descent for the investigated TP methods.

in Appendix V.B. To emphasize that the purpose of the filter in this benchmark is for TP, *not* state estimation, in what follows KF-TP refers to the Kalman filter-based benchmark, while LWPF refers to the proposed algorithm in Section II.B.

Further to the KF-TP benchmark, two different methods of generating trajectories using BADA were included as benchmark TP methods: one in which the BADA trajectory was generated at the first timestep and ‘frozen’ for the remainder of the trajectory and a second implementation where BADA was re-initialized at the measured flight level at each timestep. The BADA trajectory at $t = 0$ was used to quantify the level of misspecification between existing deterministic TP methods and real-world trajectories. Re-initializing BADA every timestep provides a benchmark adaptive TP method that adjusts the initial altitude of the aircraft using the last observation, but does not assimilate any aspect of aircraft performance.

Figure 2 compares the performance of the various TP methods, as quantified by the mean absolute error (MAE). The results are tabulated in Table 8. As expected, the three adaptive TP methods greatly outperform the BADA trajectory at $t = 0$. Due to local constraints and procedures, as well as other aleatoric and epistemic uncertainties, there is significant mis-specification of aircraft speed profiles in BADA, leading to large errors in the flown distance, particularly in climb. The error bars for the various BADA based methods are significantly wider than for the KF-TP and LWPF approaches suggesting that BADA does not have the flexibility to account for the range of aircraft performance observed in the test dataset. The KF-TP and LWPF based methods are more accurate than the two benchmarks using BADA. Predictions of descent are generally less accurate in the KF-TP and LWPF models compared to climb, which is understandable given that descents are heavily conditioned on procedural constraints, which are not explicitly modeled here.

From Figure 2 and Table 8 it can be seen that the LWPF has the lowest MAE for both the estimated time and flown distance of the investigated methods. We define the flown distance as the integrated TAS over the trajectory, to correct for wind effects. The LWPF approach has time estimation errors 46.3% and 64.7% lower, and distance errors 48.8% and 70.1% lower for climb and descend than the baseline KF-TP method. To gain more insight into this result the MAE for the KF-TP approach is compared against that of the LWPF method by aircraft type in Figure 3 and Table 9. Figure 4 provides another visualisation of the data, with the marker size indicating the number of radar blips in the test dataset (recall that the models were used to predict top of climb/bottom of descent after every new observation). Points in the

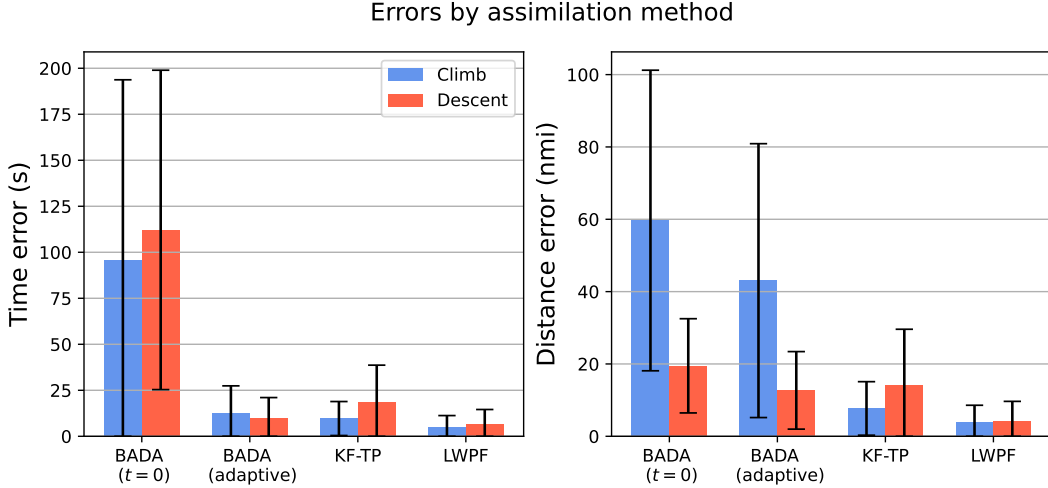


Fig. 2 Comparison of the MAE in predicting the time and location of top of climb/bottom of descent between the investigated TP methods.

top right indicate that the LWPF MAE is lower than that of the KF-TP, while the bottom left quadrant indicates the MAE is lower for the KF-TP for both time and distance flown. From the figures and table it is clear that the MAE for jet aircraft is generally lower than that for turboprops (DH8D, F2TH, and PC12). The percentage difference between the LWPF and KF-TP is greatest for the largest passenger jet types such as the A320, B738, and E190, suggesting that the performance of the particle filter is strongly correlated with the diversity of the particles in its prior, that is the representation of that aircraft type in the data. This observation would seem to be supported by the results for the B78X, which is expected to have similar performance characteristics to the A320 and B738, but with significantly fewer aircraft in the training dataset (see Table 7). Comparing the B78X errors to the B738, the B78X error is consistently greater for the LWPF in Table 9, whereas the KF-TP error for the B78X is either comparable to, or in several cases better than, the B738. Prediction of the DH8D and PC12 turboprops in descent is more accurate for the KF-TP, but not for the F2TH. The F2TH and PC12 occur roughly as frequently as one another, suggesting that the reasons for the relatively poor performance of the LWPF is not necessarily explained by insufficient numbers of particles in the training set. Turboprop aircraft frequently descend at a fixed rate of descent, which can be better approximated by the fixed ROCD trajectory generation model of the KF-TP [11].

Finally, Figure 5 plots the performance of the methods for a set of climbing flights in the test dataset. Similarly, Figure 6 displays trajectories for these aircraft types in descent. One flight from the A320, C56X, and PC12 datasets was chosen for visualisation to give examples of aircraft with markedly different (physical) performance characteristics. The A320 is a large passenger jet that frequently occurs in UK airspace, the C56X is a smaller business jet, and the PC12 an example of a single engined turboprop aircraft that is the least common of the investigated aircraft types. Each sub-figure is split into left and right panels, with the left panels plotting aircraft altitude against time and the right panel displaying TAS against time. In the left panels, the mean predicted trajectory from the particles in the LWPF are plotted every one or two minutes and compared to the generated KF-TP trajectories. Credible intervals of 2σ are generated using the arrival time/flown distance at intervals of 500ft for the ensemble of trajectories predicted by the LWPF. In the right panels the TAS estimated by the LWPF (blue) and KF-TP (red) are compared to observation data and the predicted TAS from BADA.

With the exception of the A320 in climb in Figure 5a, there is often significant misspecification of the BADA speed profile compared to the observed data. In the case of the climbs in Figure 5b and 5c and descent in Figure 6c the discrepancy in TAS profile appears consistent throughout the trajectory. In other trajectories the discrepancy is more complex: the A320 climb in Figure 5a performs the CAS-Mach transition around 30,000 ft, which is much lower than the transition altitude in the BADA model. In Figures 6a and 6b the BADA TAS profile is expected to be constant above the tropopause (around 36,000 ft), accelerating between the tropopause and CAS-Mach transition, before decreasing with altitude during the subsequent descent. Although the BADA TAS profile can often be significantly misspecified compared to the real trajectory data, the plots demonstrate how the LWPF is sufficiently flexible to adjust its estimate of the state despite the range in aircraft performance observed. The state estimate of both the KF-TP and LWPF closely

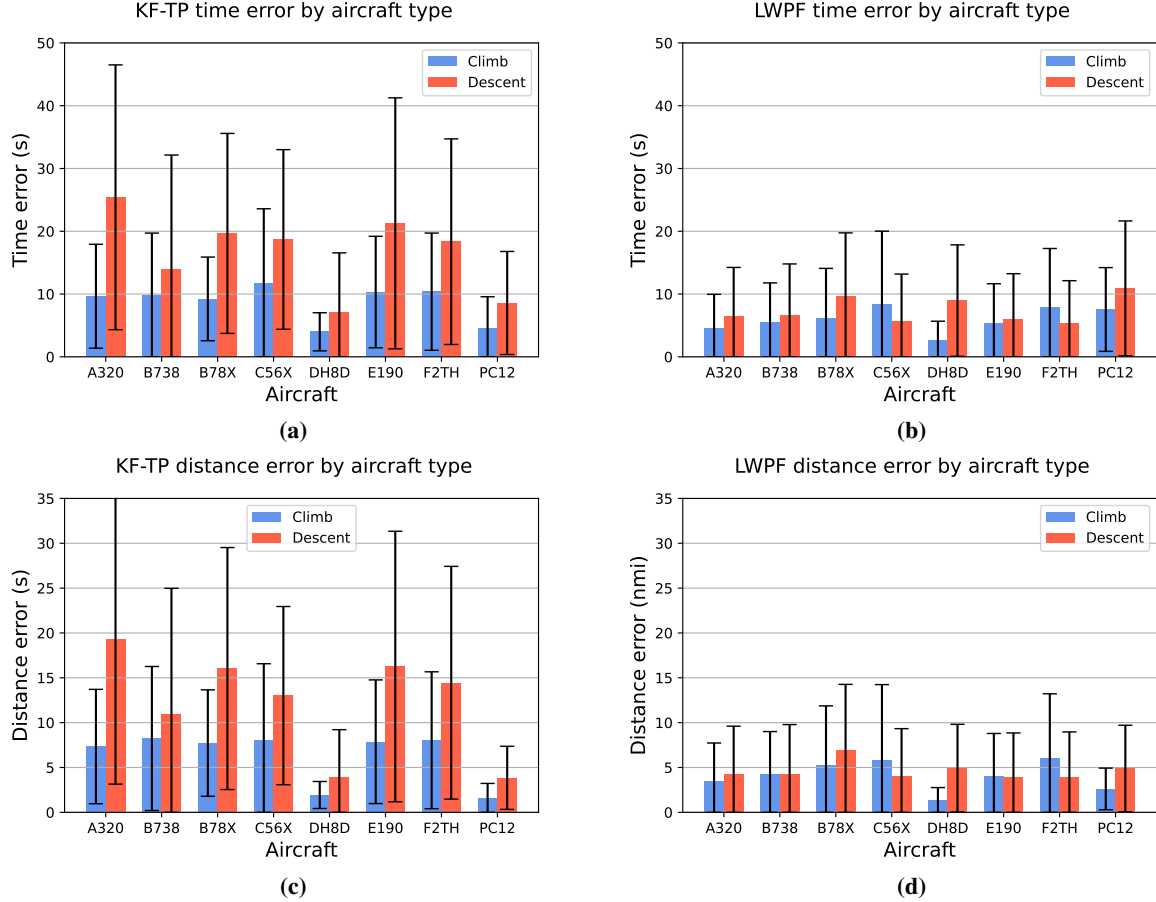


Fig. 3 KF-TP MAE compared to LWPF, displayed by aircraft type.

tracks the observed Mode S radar, Figure 6b shows an example of the LWPF re-initialising due to the particles becoming too concentrated to capture the changing descent mode of the C56X trajectory around 400s. The KF-TP tracks the state more closely as the Kalman filter can continuously adjust to new observations, while state estimation in the particle filter is dependent on the particles in the filter being sufficiently diverse to capture the true state of the aircraft.

Aircraft type	MAE time error (s)				MAE distance error (nmi)			
	Climb		Descent		Climb		Descent	
	LWPF	KF-TP	LWPF	KF-TP	LWPF	KF-TP	LWPF	KF-TP
A320	4.57	6.53	6.44	20.36	3.54	5.23	4.26	15.73
B738	5.57	9.85	6.64	13.91	4.26	8.23	4.30	10.92
B78X	6.27	5.58	9.07	14.78	5.31	5.19	6.71	12.13
C56X	8.29	9.13	5.81	13.77	5.78	6.45	4.04	9.56
DH8D	2.71	3.98	8.96	7.05	1.31	1.93	4.92	3.93
E190	5.33	7.72	6.00	16.67	4.05	6.14	3.95	12.91
F2TH	7.42	8.29	5.10	14.41	5.67	6.69	3.54	11.43
PC12	7.62	6.34	10.30	6.53	2.64	2.25	4.64	2.96

Table 9 Comparison of KF-TP errors to the LWPF by aircraft type.

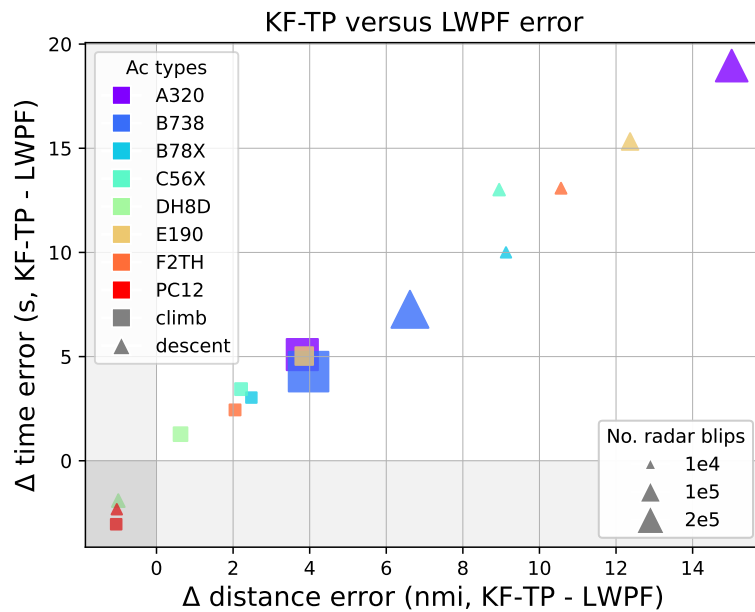


Fig. 4 The difference in errors between the KF-TP and LWPF filtering methods, per aircraft type, with marker size determined by number of radar blips in the test dataset for that aircraft type.

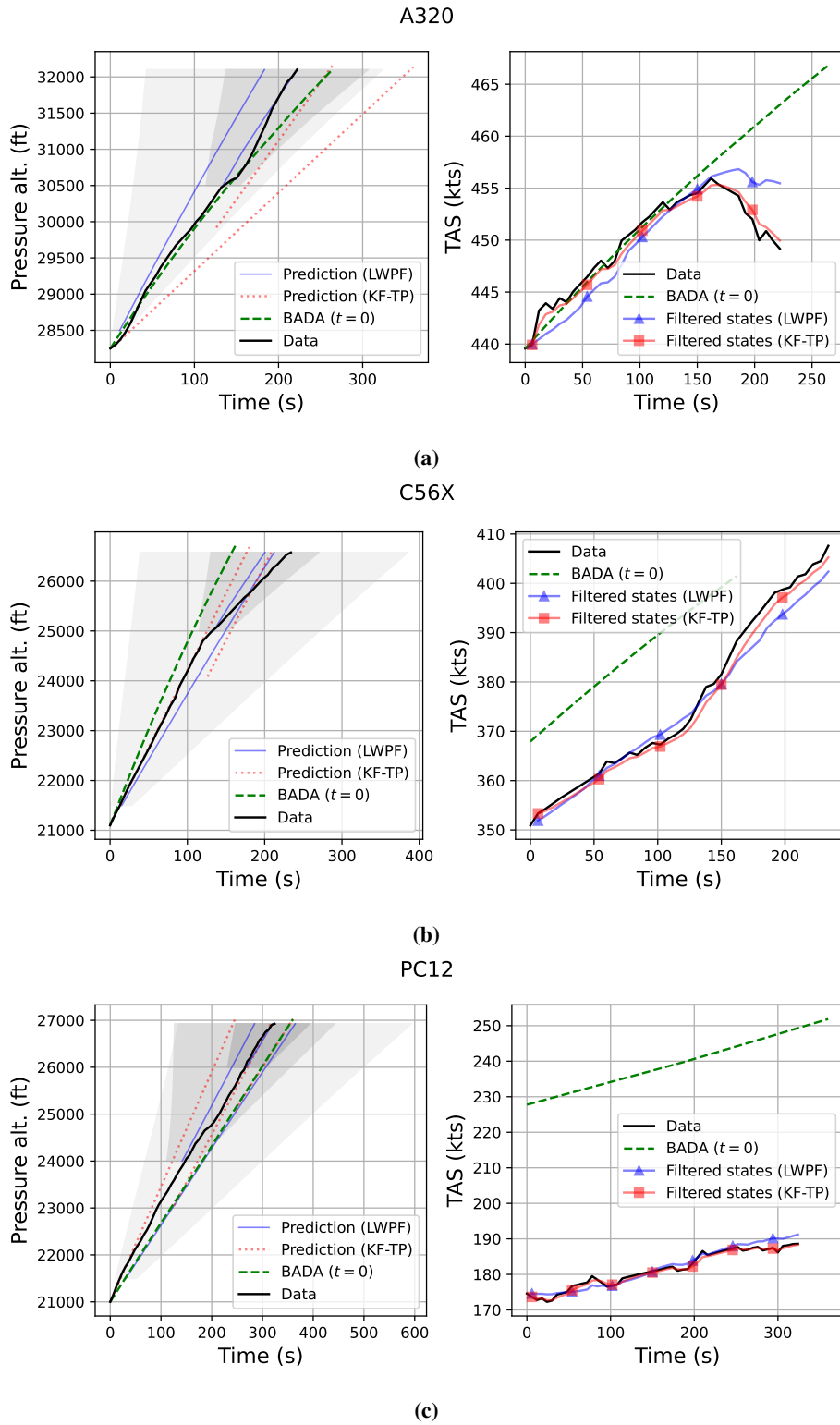
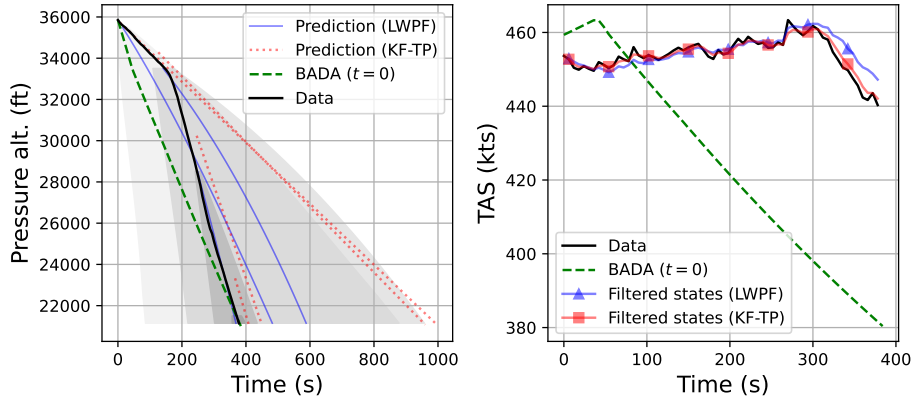


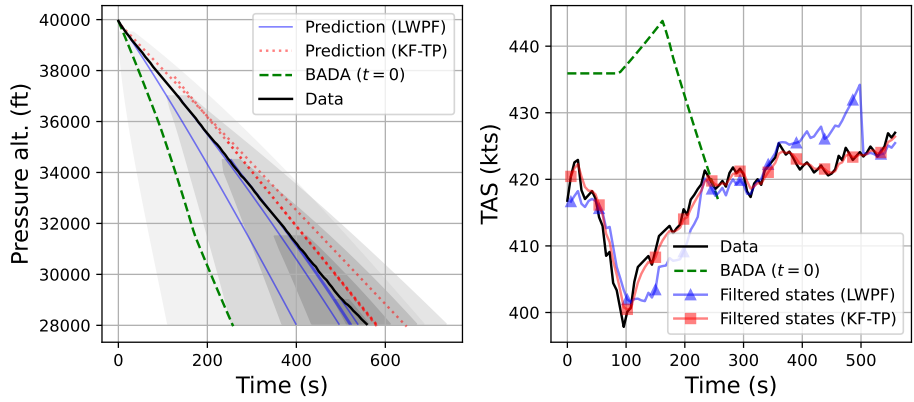
Fig. 5 Climbing trajectories sampled from the test dataset, compared to TPs from the investigated methods. Panels on the left display altitude against time, while those on the right indicate TAS against time.

A320



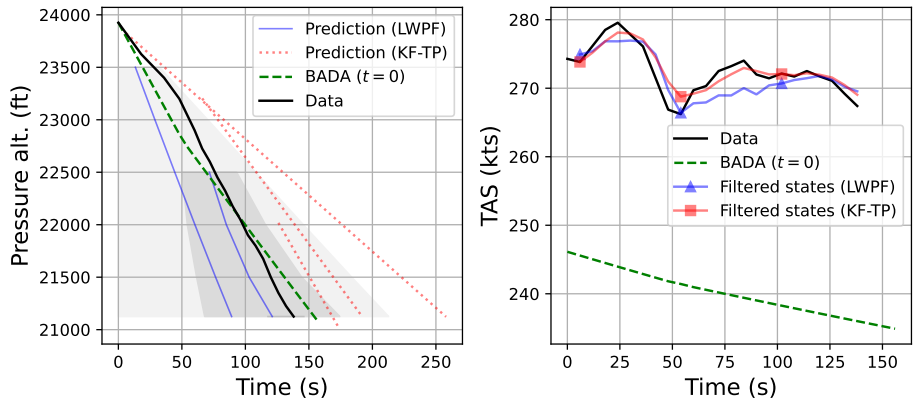
(a)

C56X



(b)

PC12



(c)

Fig. 6 Descending trajectories sampled from the test dataset, compared to TPs from the investigated methods. Panels on the left display altitude against time, while those on the right indicate TAS against time.

V. Discussion

A novel method for adaptive TP has been presented in this paper. The method is based on a particle filter that uses a set of learned LSSMs as a prior for aircraft dynamics. The model has demonstrated increased accuracy in climb and descent compared to a set of benchmarks that reflect current state of the art TP methods. The proposed method offered time predictions that were 46.3% and 64.7% lower than the nearest benchmark for climb and descent respectively. Beyond the presented application to adaptive TP, TP using LSSMs offers a fast surrogate for BADA, an industry standard TP method that is based around the numerical solution of a PDE, by a factor of 5.26 in climb and 8.11 in descent.

The results presented in this paper are promising, but they also highlight several areas where the method could be improved with future work. Firstly, performance of the method clearly degrades for aircraft types with relatively low numbers of training data. This might be mitigated through a transfer learning approach, in which LSSMs from other aircraft types with similar dynamics can be pooled. The LSSMs model ROCD and TAS jointly. However, there are instances, such as descending turboprops, where better results can be obtained with a simpler TP model. Such cases may well be better handled by an even simpler, approach using polynomials as TP surrogates. Finally, although confidence intervals were plotted in Figures 5 and Figure 6 for illustrative purposes, this paper has been concerned with validating the accuracy of the proposed approach, rather than assessing the calibration of the probabilistic bounds. Further work will develop this aspect of the method, using the frequency with which observed data points lie outside of the predicted bounds as a diagnostic tool that can be used to further improve the model and assist the user to define the contours of its trustworthiness.

Appendix

A. Linearisation of the BADA equations

Usually, a two-dimensional system whose dynamics are described by:

$$\dot{\mathbf{x}} = \begin{bmatrix} f(\mathbf{x}, \mathbf{u}) \\ g(\mathbf{x}, \mathbf{u}) \end{bmatrix}, \quad (15)$$

where $f(\cdot)$ and $g(\cdot)$ are non-linear functions, may be linearized by taking a Taylor series around an operating point, \mathbf{x}_e . Using the definition of the state in Section II.A the expansion for $f(\cdot)$ is:

$$f(h, V_{TAS}) \approx f(h_e, V_e) + \frac{\partial f}{\partial h} \bigg|_{h_e, V_e} \Delta h + \frac{\partial f}{\partial V_{TAS}} \bigg|_{h_e, V_e} \Delta V_{TAS} + \frac{\partial f}{\partial u} \bigg|_{h_e, V_e} \Delta u, \quad (16)$$

where $\mathbf{x}_e = [h_e, V_e]^\top$ denotes the operating point. Using an equivalent expression for $g(\cdot)$ the continuous time linear system may be written as:

$$A = \begin{bmatrix} \frac{\partial f}{\partial h} \bigg|_{h_e, V_e} & \frac{\partial f}{\partial V_{TAS}} \bigg|_{h_e, V_e} \\ \frac{\partial g}{\partial h} \bigg|_{h_e, V_e} & \frac{\partial g}{\partial V_{TAS}} \bigg|_{h_e, V_e} \end{bmatrix} \text{ and } B = \begin{bmatrix} \frac{\partial f}{\partial u} \bigg|_{h_e, V_e} \\ \frac{\partial g}{\partial u} \bigg|_{h_e, V_e} \end{bmatrix}. \quad (17)$$

$f(h, V_{TAS})$ is the equivalent of (1). It is natural to treat the aircraft thrust, T_{HR} , as the external forcing term. From equations (3.7-1) and (3.7-2) in Nuic et al. [1] it is apparent that T_{HR} is a function of h for jet aircraft and h and V_{TAS} for turboprop aircraft such as the DH8D and PC12. In other words, the forcing is a function of the state variables and not time. The TAS of a climbing aircraft in BADA in the standard atmosphere can be well approximated as a cubic function of h (see Figure 7), i.e.:

$$V_{TAS} = \lambda_1 h^3 + \lambda_2 h^2 + \lambda_3 h + \lambda_4, \quad (18)$$

with:

$$g(h, V_{TAS}) = (3\lambda_1 h^2 + 2\lambda_2 + \lambda_3)f(h, V_{TAS}), \quad (19)$$

through the chain rule. The forcing in $f(h, V_{TAS})$ rescaled by a quadratic function of h in (19). Properly speaking the forcing should be absorbed into A and B set to zero as it is only a function of state parameters. However, it was found that the fit to data was better when a constant forcing with two separate constant forcing parameters was learned as the models had greater flexibility, hence $B \in \mathbb{R}^2$ in this paper.

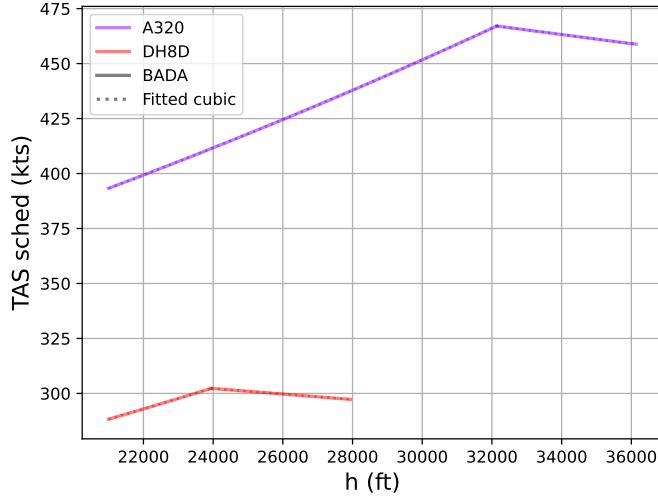


Fig. 7 Fitting cubic functions to TAS as a function of h , above and below transition point, for the A320 and DH8D as examples of jet and turboprop aircraft respectively.

B. Kalman filter benchmark

The Kalman filter is a standard approach for state estimation that has been successfully applied in many domains. It is therefore a logical benchmark to measure an algorithm that performs state estimation against. However, the studied application of adaptive TP requires both state estimation *and* trajectory prediction. We propose the following benchmark for adaptive TP that is based around a Kalman filter, which we denote the KF-TP. We define a three-dimensional state that contains the ROCD, TAS and altitude of an aircraft. All three of these quantities are returned by Mode S radar returns. A simplistic trajectory prediction is performed by assuming the aircraft will continue to climb or descend at the filtered ROCD and TAS.

Some quantities in the Kalman filter must be set by the user such as the initial state uncertainty matrix, P , and the process noise Q . In what follows these matrices take the following structure:

$$P = \alpha_p I_3 \text{ and } Q = \alpha_q I_3, \quad (20)$$

where I_3 is the 3×3 identity matrix. The scalars α_p and α_q were scalars that were set by performing a sweep over the validation dataset for different values of these hyperparameters. Precise values for the measurement noise covariance, R , are not publicly available. For the purposes of this paper the error covariances were set reasonable estimates of 100 ft/min for the ROCD, 2.5 knots for TAS, and 100 ft. Additionally, an external forcing term was included in the state prediction step of the filter of:

$$\Phi_B = \begin{bmatrix} 0 \\ \alpha_b \\ 0 \end{bmatrix}, \quad (21)$$

where α_b was a forcing applied to the aircraft altitude, this is consistent with the scaling of the fitted LSSMs in Section II.A. Sweeps were performed over the validation set to determine the best choices of hyperparameters for the KF-TP. The first swept over values of α_p and α_q , while holding the forcing constant, with $\alpha_b = \pm 1500\delta t/60$, where $\delta t = 6$ s refers to the timestep between radar blips. These weights can be interpreted as a constant increase or decrease in altitude per timestep.

Table 10 tabulates the results of this sweep. The ‘number of points’ column indicates the numbers of blips in the validation set for which a trajectory was successfully generated. A successfully generated trajectory has an absolute ROCD of greater than or equal to 500 ft/min for all radar blips. This reflects that there is a legal minimum climb or

descent rate of 500 ft/min in UK airspace one a clearance for climb or descent has been issued by an air traffic controller. This sweep demonstrated that the performance of the filter was relatively insensitive to the choice of α_q .

A second sweep was performed over α_b , with $\alpha_p = 1e5$ and $\alpha_q = 1$, following the results in Table 10. The results of this sweep are presented in Table 11. Best results across the B738 and DH8D were obtained for $\alpha_b = 500\text{ft/min}$ in climb, with the results for descent more inconsistent between the two aircraft types. The results in Section IV were obtained using $\alpha_b = 500\text{ft/min}$ in climbs and $\alpha_b = 1500\text{ft/min}$ in descents.

C. Sweep over number of particles

Table 12 displays how the performance of the LWPF varies with number of particles in the filter. As above, the sweep was performed over the B738 and DH8D aircraft types as examples of aircraft with both significantly different performance and different numbers of trajectories in the training and validation datasets. As might be expected, performance improves for the B738 as more particles are included in the filter. However, the reduction in MAE diminishes with particle size, hence a particle size of 400 was chosen as a compromise between improved MAE in the validation set and the computational cost associated with generating trajectories for each particle. The trend is more complex for the DH8D, where the MAE is lower for lower numbers of particles. However, at the same time the failure rate for the trajectory generation is much higher for these particles, for instance 72.6% of trajectories generated by the filter with 50 particles have an absolute ROCD of less than 500 ft/min. Given that there was no clear trend for the DH8D and to ensure that the failure rate was on the order of 5% or below, a particle size of 400 was used across all aircraft types.

P scaling	Q scaling	Aircraft type	Climb				Descent			
			Time error (s)	Distance error (nmi)	Failure rate	Number of points	Time error (s)	Distance error (nmi)	Failure rate	Number of points
100000	0.0001	B738	9.82	8.30	0.00	144156	13.13	10.21	0.01	127224
100000	0.01	B738	9.75	8.07	0.00	144156	12.93	9.92	0.01	127224
100000	1.00	B738	8.42	6.82	0.00	144157	10.90	8.17	0.01	127219
10000	0.0001	B738	9.82	8.30	0.00	144156	13.14	10.22	0.01	127220
10000	0.01	B738	9.76	8.07	0.00	144156	12.95	9.93	0.01	127219
10000	1.00	B738	8.42	6.82	0.00	144157	10.91	8.18	0.01	127216
1000	0.0001	B738	9.82	8.31	0.00	144152	13.26	10.33	0.01	127177
1000	0.01	B738	9.76	8.07	0.00	144152	13.07	10.04	0.01	127176
1000	1.00	B738	8.42	6.82	0.00	144153	11.00	8.26	0.01	127175
100	0.0001	B738	9.88	8.35	0.00	144111	14.49	11.33	0.01	126727
100	0.01	B738	9.82	8.11	0.00	144112	14.28	11.02	0.01	126725
100	1.00	B738	8.43	6.82	0.00	144109	11.87	8.97	0.01	126745
1	0.0001	B738	14.72	11.62	0.01	142882	42.15	30.80	0.17	106589
1	0.01	B738	14.34	11.21	0.01	142947	38.83	28.07	0.16	107778
1	1.00	B738	9.32	7.42	0.00	143740	16.13	12.00	0.06	120026
100000	0.0001	DH8D	5.10	2.45	0.00	8044	7.05	3.85	0.00	4708
100000	0.01	DH8D	5.08	2.43	0.00	8044	7.02	3.83	0.00	4708
100000	1.00	DH8D	3.80	1.83	0.00	8044	5.75	3.17	0.00	4708
10000	0.0001	DH8D	5.10	2.45	0.00	8044	7.05	3.85	0.00	4708
10000	0.01	DH8D	5.08	2.43	0.00	8044	7.03	3.84	0.00	4708
10000	1.00	DH8D	3.80	1.83	0.00	8044	5.76	3.17	0.00	4708
1000	0.0001	DH8D	5.11	2.45	0.00	8044	7.16	3.92	0.00	4708
1000	0.01	DH8D	5.09	2.44	0.00	8044	7.14	3.90	0.00	4708
1000	1.00	DH8D	3.80	1.83	0.00	8044	5.86	3.23	0.00	4708
100	0.0001	DH8D	5.18	2.49	0.00	8044	8.18	4.50	0.00	4708
100	0.01	DH8D	5.16	2.47	0.00	8044	8.15	4.49	0.00	4708
100	1.00	DH8D	3.85	1.86	0.00	8044	6.85	3.80	0.00	4708
1	0.0001	DH8D	7.01	3.36	0.00	8044	24.90	13.79	0.01	4659
1	0.01	DH8D	6.95	3.34	0.00	8044	24.62	13.64	0.01	4660
1	1.00	DH8D	4.43	2.14	0.00	8044	15.86	8.81	0.01	4684

Table 10 Sweep of Kalman filter parameters over the validation datasets for P and Q scalings.

B scaling	Aircraft type	Climb				Descent			
		Time error (s)	Distance error (nmi)	Failure rate	Number of points	Time error (s)	Distance error (nmi)	Failure rate	Number of points
2000	B738	9.45	7.56	0.00	144157	10.65	7.84	0.01	127239
1500	B738	8.42	6.82	0.00	144157	10.90	8.17	0.01	127219
1000	B738	7.67	6.27	0.00	144152	11.51	8.72	0.01	127200
500	B738	7.49	6.14	0.00	144148	12.50	9.47	0.01	127165
0	B738	7.71	6.29	0.00	144144	13.70	10.33	0.01	127142
2000	DH8D	5.17	2.47	0.00	8044	5.97	3.26	0.00	4708
1500	DH8D	3.80	1.83	0.00	8044	5.75	3.17	0.00	4708
1000	DH8D	2.38	1.17	0.00	8044	6.34	3.51	0.00	4708
500	DH8D	2.34	1.14	0.00	8044	7.93	4.41	0.00	4708
0	DH8D	3.61	1.73	0.00	8044	10.16	5.63	0.00	4708

Table 11 Sweep of Kalman filter parameters over the validation datasets for the B scaling.

Number of particles	Aircraft type	Climb				Descent			
		Time error (s)	Distance error (nmi)	Failure rate	Number of points	Time error (s)	Distance error (nmi)	Failure rate	Number of points
50	B738	6.43	5.09	0.01	143437	7.90	5.08	0.00	127611
100		5.90	4.62	0.00	144171	7.41	4.82	0.00	128068
200		5.59	4.33	0.00	144193	6.94	4.53	0.00	128136
400		5.44	4.18	0.00	144281	6.67	4.33	0.00	128207
800		5.38	4.11	0.00	144292	6.53	4.26	0.00	128231
1600		5.33	4.06	0.00	144297	6.41	4.17	0.00	128167
3200		5.34	4.06	0.00	144297	6.35	4.15	0.00	128243
50	DH8D	3.74	1.77	0.00	8039	4.41	2.41	0.73	1288
100		3.61	1.71	0.00	8044	6.13	3.37	0.44	2634
200		3.68	1.74	0.00	8044	7.61	4.17	0.22	3657
400		3.63	1.72	0.00	8044	9.21	5.07	0.05	4470
800		3.62	1.71	0.00	8044	9.52	5.23	0.01	4650
1600		3.65	1.73	0.00	8044	9.52	5.24	0.00	4700

Table 12 Sweep over particle sizes in the LWPF on the validation dataset

Acknowledgments

The authors would like to thank Dr. Lawrence Bull, Research Fellow at the University of Glasgow, for providing useful insight on particle filtering.

Funding Sources

The work described in this paper is primarily funded by the grant “EP/V056522/1: Advancing Probabilistic Machine Learning to Deliver Safer, More Efficient and Predictable Air Traffic Control” (aka Project Bluebird), an EPSRC Prosperity Partnership between NATS, The Alan Turing Institute, the University of Exeter, and the University of Cambridge.

References

- [1] Nuic, A., “User manual for the Base of Aircraft Data (BADA) revision 3.10,” *Atmosphere*, Vol. 2010, 2010, p. 001. URL <http://maartenuijtdehaag.com/bada310-user-manual.pdf>.
- [2] Bastas, A., Kravaris, T., and Vouros, G. A., “Data driven aircraft trajectory prediction with deep imitation learning,” *arXiv*, 2020. URL <https://arxiv.org/abs/2005.07960>.
- [3] Pang, Y., Zhao, X., Yan, H., and Liu, Y., “Data-driven trajectory prediction with weather uncertainties: A Bayesian deep learning approach,” *Transportation Research Part C: Emerging Technologies*, Vol. 130, 2021, p. 103326. URL <https://doi.org/10.1016/j.trc.2021.103326>.
- [4] Silvestre, J., Mielgo, P., Bregon, A., Martínez-Prieto, M. A., and Álvarez Esteban, P. C., “Multi-Route Aircraft Trajectory Prediction Using Temporal Fusion Transformers,” *IEEE Access*, Vol. 12, 2024, pp. 174094–174106. URL <https://ieeexplore.ieee.org/abstract/document/10577632>.
- [5] Chen, Y., Sun, J., Lin, Y., Gui, G., and Sari, H., “Hybrid N-Inception-LSTM-Based Aircraft Coordinate Prediction Method for Secure Air Traffic,” *IEEE Transactions on Intelligent Transportation Systems*, Vol. 23, No. 3, 2022, pp. 2773–2783. URL <https://doi.org/10.1109/TITS.2021.3095129>.
- [6] Xiang, J., and Chen, J., “Data-Driven Probabilistic Trajectory Learning with High Temporal Resolution in Terminal Airspace,” *Journal of Aerospace Information Systems*, Vol. 0, No. 0, 2025, pp. 1–11. URL <https://doi.org/10.2514/1.I011545>.
- [7] Wu, X., Yang, H., Chen, H., Hu, Q., and Hu, H., “Long-term 4D trajectory prediction using generative adversarial networks,” *Transportation Research Part C: Emerging Technologies*, Vol. 136, 2022, p. 103554. URL <https://www.sciencedirect.com/science/article/pii/S0968090X22000031>.
- [8] Ayhan, S., and Samet, H., “Aircraft Trajectory Prediction Made Easy with Predictive Analytics,” *Proceedings of the 22nd ACM SIGKDD International Conference on Knowledge Discovery and Data Mining*, Association for Computing Machinery, New York, NY, USA, 2016, pp. 21–30. URL <https://doi.org/10.1145/2939672.293969>.
- [9] Barratt, S. T., Kochenderfer, M. J., and Boyd, S. P., “Learning Probabilistic Trajectory Models of Aircraft in Terminal Airspace From Position Data,” *IEEE Transactions on Intelligent Transportation Systems*, Vol. 20, No. 9, 2019, pp. 3536–3545. URL <https://ieeexplore.ieee.org/document/8551278>.
- [10] Pepper, N., and Thomas, M., “Learning Generative Models for Climbing Aircraft from Radar Data,” *Journal of Aerospace Information Systems*, Vol. 21, No. 6, 2024, pp. 474–481. URL <https://doi.org/10.2514/1.I011359>.
- [11] Hodgkin, A., Pepper, N., and Thomas, M., “Probabilistic Simulation of Aircraft Descent via a Physics-Informed Machine Learning Approach,” 2025. URL <https://arxiv.org/abs/2504.02529>.
- [12] Anderson, D., and Lin, X. G., “A Collision Risk Model for a Crossin Track Separation Methodology,” *Journal of Navigation*, Vol. 49, No. 3, 1996, p. 337–349. URL <https://doi.org/10.1017/S0373463300013576>.
- [13] Hsu, D., “The evaluation of aircraft collision probabilities at intersecting air routes,” *The Journal of Navigation*, Vol. 34, No. 1, 1981, pp. 78–102. URL <https://doi.org/10.1017/S0373463300024279>.
- [14] Liu, W., and Hwang, I., “Probabilistic Trajectory Prediction and Conflict Detection for Air Traffic Control,” *Journal of Guidance, Control, and Dynamics*, Vol. 34, No. 6, 2011, pp. 1779–1789. URL <https://doi.org/10.2514/1.53645>.
- [15] Lymeropoulos, I., “Sequential Monte Carlo methods in air traffic management,” Ph.D. thesis, ETH Zurich, 2010. URL <https://www.research-collection.ethz.ch/bitstream/handle/20.500.11850/152184/eth-1702-02.pdf>.

[16] Wang, B., Zou, R., Mao, J., Wu, C.-L., and Xue, D., “Developing an aircraft takeoff mass estimation model based on the hybrid KMI-DNN-BI model using quick access recorder (QAR) data,” *Aerospace Science and Technology*, Vol. 158, 2025, p. 109918. URL <https://www.sciencedirect.com/science/article/pii/S1270963824010472>.

[17] Sun, J., Ellerbroek, J., and Hoekstra, J., “Modeling and inferring aircraft takeoff mass from runway ADS-B data,” *7th International Conference on Research in Air Transportation*, 2016. URL https://pure.tudelft.nl/ws/files/8929936/Sun_Ellerbroek_Hoekstra_2016_Modeling_and_Inferring_Aircraft_Takeoff_Mass_from_Runway_ADS_B_Data.pdf.

[18] Schultz, C., Thipphavong, D., and Erzberger, H., *Adaptive Trajectory Prediction Algorithm for Climbing Flights*, 2012. URL <https://arc.aiaa.org/doi/abs/10.2514/6.2012-4931>.

[19] Madyastha, V., Ravindra, V., Mallikarjunan, S., and Goyal, A., “Extended Kalman filter vs. error state Kalman filter for aircraft attitude estimation,” *AIAA Guidance, Navigation, and Control Conference*, 2011, p. 6615. URL <https://doi.org/10.2514/6.2011-6615>.

[20] Zhang, J., Wu, X.-G., and Wang, F., “Aircraft trajectory prediction based on modified interacting multiple model algorithm,” *Journal of Donghua University (English Edition)*, Vol. 32, 2015, pp. 180–184. URL https://www.researchgate.net/publication/282919671_Aircraft_trajectory_prediction_based_on_modified_interacting_multiple_model_algorithm.

[21] Lymeropoulos, I., and Lygeros, J., “Adaptive aircraft trajectory prediction using particle filters,” *AIAA Guidance, Navigation and Control Conference and Exhibit*, 2008, p. 7387. URL <https://doi.org/10.2514/6.2008-7387>.

[22] Maeder, U., Morari, M., and Baumgartner, T. I., “Trajectory Prediction for Light Aircraft,” *Journal of Guidance, Control, and Dynamics*, Vol. 34, No. 4, 2011, pp. 1112–1119. URL <https://doi.org/10.2514/1.52124>.

[23] Liu, J., and West, M., “Combined parameter and state estimation in simulation-based filtering,” *Sequential Monte Carlo methods in practice*, Springer, 2001, pp. 197–223. URL https://doi.org/10.1007/978-1-4757-3437-9_10.

[24] Pepper, N., Keane, A., Hodgkin, A., Dewi Gould, E. H., Lauritsen, L., Vlahos, C., De Ath, G., Everson, R., Cannon, R., Castro, A. S., Korna, J., Carvell, B., and Thomas, M., “A Probabilistic Digital Twin of UK En Route Airspace for Training and Evaluating AI Agents for Air Traffic Control,” *AIAA SCITECH 2026 Forum*, 2026.

[25] Nelder, J. A., and Mead, R., “A simplex method for function minimization,” *The computer journal*, Vol. 7, No. 4, 1965, pp. 308–313. URL <https://doi.org/10.1093/comjnl/7.4.308>.

[26] Mazor, E., Averbuch, A., Bar-Shalom, Y., and Dayan, J., “Interacting multiple model methods in target tracking: a survey,” *IEEE Transactions on Aerospace and Electronic Systems*, Vol. 34, No. 1, 1998, pp. 103–123. URL <https://ieeexplore.ieee.org/document/640267>.

[27] Nemeth, C., Fearnhead, P., and Mihaylova, L., “Sequential Monte Carlo methods for state and parameter estimation in abruptly changing environments,” *IEEE Transactions on Signal Processing*, Vol. 62, No. 5, 2013, pp. 1245–1255. URL <https://ieeexplore.ieee.org/abstract/document/6692890>.